Atmos. Chem. Phys., 11, 10071–10084, 2011
www.atmos-chem-phys.net/11/10071/2011/
doi:10.5194/acp-11-10071-2011

Atmospheric Chemistry and Physics

TransCom continuous experiment: comparison of ^{222}Rn transport at hourly time scales at three stations in Germany

S. Taguchi[1], R. M. Law[2], C. Rödenbeck[3], P. K. Patra[4], S. Maksyutov[5], W. Zahorowski[6], H. Sartorius[7], and I. Levin[8]

[1]National Institute of Advanced Industrial Science and Technology, Tsukuba, Japan
[2]Centre for Australian Weather and Climate Research, CSIRO Marine and Atmospheric Research, Aspendale, Victoria, Australia
[3]Max-Planck-Institute for Biogeochemistry, Jena, Germany
[4]Frontier Research Center for Global Change/JAMSTEC, Yokohama, Japan
[5]National Institute of Environmental Studies, Tsukuba, Japan
[6]Australian Nuclear Science and Technology Organization, Menai, New South Wales, Australia
[7]Federal Office for Radiation Protection, Freiburg, Germany
[8]Institut für Umweltphysik, University of Heidelberg, Germany

Received: 24 June 2011 – Published in Atmos. Chem. Phys. Discuss.: 6 July 2011
Revised: 21 September 2011 – Accepted: 27 September 2011 – Published: 6 October 2011

Abstract. Fourteen global atmospheric transport models were evaluated by comparing the simulation of ^{222}Rn against measurements at three continental stations in Germany: Heidelberg, Freiburg and Schauinsland. Hourly concentrations simulated by the models using a common ^{222}Rn-flux without temporal variations were investigated for 2002 and 2003. We found that the mean simulated concentrations in Heidelberg are related to the diurnal amplitude of boundary layer height in each model. Summer mean concentrations simulated by individual models were negatively correlated with the seasonal mean of diurnal amplitude of boundary layer height, while in winter the correlation was positive. We also found that the correlations between simulated and measured concentrations at Schauinsland were higher when the simulated concentrations were interpolated to the station altitude in most models. Temporal variations of the mismatch between simulated and measured concentrations suggest that there are significant interannual variations in the ^{222}Rn exhalation rate in this region. We found that the local inversion layer during daytime in summer in Freiburg has a significant effect on ^{222}Rn concentrations. We recommend Freiburg concentrations for validation of models that resolve local stable layers and those at Heidelberg for models without this capability.

Correspondence to: S. Taguchi
(s.taguchi@aist.go.jp)

1 Introduction

Source-receptor relationships for atmospheric compounds, like gases and fine particles, are one of the tools to understand and to manage air quality. A set of source-receptor relationships forms a response matrix, or Jacobian matrix, and plays a central role in making an inverse estimate of sources and sinks of compounds. Global atmospheric transport models have been developed to describe this relationship, and include various pathways. Some examples of these pathways are diffusion in the atmospheric boundary layer (ABL), transport by convection and synoptic disturbances in the free troposphere, interactions with cloud and rain droplets, chemical reactions, dry and wet deposition to the surface. There is a variety of realism in the modeling of each process. Validation of the source-receptor relationship is required for effective application of emission control, both technically and politically.

A group dealing with the inverse modeling of sources and sinks of carbon dioxide conducted an inter-comparison project of global atmospheric transport models (TransCom-continuous) focused on diurnal (Law et al., 2008) and synoptic (Patra et al., 2008) timescales (http://www.purdue.edu/transcom). It was found that the simulated diurnal amplitudes of CO_2 have a weak relationship with vertical resolution in the models. The differences between models in how near-surface mixing was simulated were as important as the vertical resolution. It was also found that the correlation of simulated and measured daily CO_2 is related to the distance of the model sampling location from the measurement

location. Two factors are suggested to contribute to lower correlations for larger distances: the spatial heterogeneity of surface fluxes in the vicinity of the site and the spatial scale of concentrations corresponding to meteorological systems. As for vertical levels, an appropriate level for mountain sites for comparison with the observation was not apparent. The aim of observations at mountain sites is to measure background, non-polluted air but the observed concentrations (and modelled concentrations) at a fixed level may not always satisfy that criterion. Therefore the model evaluations could not be conclusive. ^{222}Rn was included in the TransCom simulations as one of their model evaluation compounds.

^{222}Rn is a noble gas emanating from soils and rocks containing ^{226}Ra. It is exhaled from the soil air to the atmosphere and decays with a half-life of 3.824 days. Activity concentrations are measured from its radioactive decay or from the decay of its progenies collected on filters. ^{222}Rn exhalation rate from the ground is a function of the amount of ^{226}Ra in the soil material, the grain size of the soil, and the water content of the soil at a chamber measurement scale (Nazaroff, 1992), and it is a function of water table depth at regional scales (Levin et al., 2002). Measurement of radioactivity in the lower part of the ABL was made on activated charcoal at 0.97 m, 5.72 m, 23.8 m and 39.9 m level at Argonne National Laboratory (Moses et al., 1960). Other measurements were made using progenies of ^{222}Rn on aerosol collected on filters at 1 m, 15 m, 30 m and 100 m level at the plateau of Saclay in the outskirts of Paris (Servant, 1966). Vertical profiles within the ABL have recently been measured with gliders (Williams et al., 2011). They all showed large vertical gradients during night and almost constant concentrations in the vertical down to 1 m during daytime.

The vertical gradient of ^{222}Rn between Freiburg (276 m a.m.s.l. (above mean sea level)) and Schauinsland (1205 m a.m.s.l.) has been used to evaluate atmospheric transport models (Olivié et al., 2004; Chevillard et al., 2002) because these two sites are generally within the same model grid-box horizontally, but Freiburg is a low-level site and Schauinsland is a mountain site. The vertical gradient of ^{222}Rn in the ABL in an open flat area is the result of accumulation from soil exhalation and dilution of ^{222}Rn due to ventilation of ABL air with free troposphere air caused by the diurnal change of the ABL height. If we assume the area where tower observations and glider measurements were made to be open and flat, the ratio of concentrations in Freiburg and concentrations at Schauinsland are expected to approach one if the ABL top exceeds the height of the Schauinsland mountain ridge. Observed concentrations in Freiburg are twice as high compared to Schauinsland even if the ABL height rises above the Schauinsland level. Two types of boundary layer schemes, local and non-local, were evaluated in the TM3 chemistry transport model combined with diffusion coefficients archived in the reanalysis process (Olivié et al., 2004). Local schemes simulate vertical diffusion based on local gradients of wind and virtual temperature whereas non-local schemes take into account counter-gradient transport due to eddies (Troen and Mahrt, 1986; Holtslag and Boville, 1993; Lock et al., 2000). All boundary layer schemes, including local and non-local schemes, produced a vertical gradient comparable to the measured one if the model level for comparison is selected with special care for the site effects of the stations (Chevillard et al., 2002). Temperature of the site was used to include the site effect. The Schauinsland Ozone Precursor Experiment (SLOPE) conducted in June 1996 (Kalthoff et al., 2000; Fiedler et al., 2000) demonstrated the formation of a cold air pool and the build-up of local low level inversions during daytime on clear summer days in this area; this feature has not been taken into account in the evaluations of low resolution models.

Various ^{222}Rn flux distributions have been proposed including an exhalation rate distribution based on multiple factors, such as radium content in the soil, grain size of the soil (Schery and Wasiolek, 1998) a flux distribution with a decrease with latitude north of 30° N (Connen and Robertson, 2002), and a spatially and temporally resolved exhalation rate map over Europe using gamma dose rate (Szegvary et al., 2007, 2009). A flux distribution over ocean was estimated using radium content in the sea-water and wind speed dependency of the gas transfer velocity between air and the sea (Schery and Huang, 2004). Temporal variations of the ^{222}Rn flux are also important. The flux of ^{222}Rn has been measured on clay and sandy soils in West Germany for one year (Dörr and Münnich, 1990). The flux from clay soil was found to have $\pm 36\,\%$ maximum deviations from the long term mean with higher fluxes in summer than winter. The flux showed no seasonal variations from sandy soil. A seasonally varying flux with minimum values of 12.2 mBq m^{-2} s^{-1} in January and maximum values of 19.5 mBq m^{-2} s^{-1} in August is usually assumed in the radon-tracer method for estimation of greenhouse gas emissions in the Heidelberg catchment (Schmidt et al., 2001; Levin et al., 2003; Hammer and Levin, 2009). However, in transport model evaluations , including the TransCom simulations analysed for this paper, constant emissions from continental surfaces of 1 atom cm^{-2} s^{-1} (=1.66 $\times$ 10^{-20} mol m^{-2} s^{-1}, 21.0 mBq m^{-2} s^{-1}) have mostly been used (Heimann and Keeling, 1989; Allen et al., 1996; Mahowald et al., 1997; Jacob et al., 1997; Stockwell, 1998; Dentener et al., 1999; Chevillard et al., 2002; Taguchi et al., 2002; Josse et al., 2004; Olivié et al., 2004; Considine et al., 2005; Donner et al., 2007; Zhang et al., 2008). The use of a constant flux from continental surfaces definitely introduces some degree of mismatch between simulation and measurements.

We have attempted to evaluate individual model output submitted to the TransCom continuous experiment by means of ^{222}Rn along with boundary layer height (BLH). A total of 25 models submitted results. We used only the 14 models that submitted both ^{222}Rn activity concentrations and explicit BLH.

^{222}Rn observations and a set of reference BLH are described in Sect. 2. Participating models and specifications of ^{222}Rn experiments are described in Sect. 3. The ensemble mean of model outputs as well as individual model output are compared with the observations in Sect. 4. A relationship between mean concentrations and BLH, and an estimate of temporal variations of emissions are discussed in Sect. 5. The results are summarized in Sect. 6.

2 Measurements

2.1 Hourly concentration measurements of ^{222}Rn

We used data from three inland stations in Germany as shown in Fig. 1. Freiburg (47°59′56" N, 7°50′52" E, 27 6 m a.m.s.l.) is located in the Rhine valley in southern Germany. The measurement is made at 8 m above the ground. The monitoring site at Schauinsland (47°54′57" N, 7°54′29", 1205 m a.m.s.l.) is located about 12 km south of Freiburg on the saddle of a hill (1284 m). Hourly measurements at Freiburg and Schauinsland are performed by the Federal Office for Radiation Protection, Germany. The observational site of Heidelberg (49°24′37" N, 8°42′23" E, 116 m a.m.s.l.) is also located in the upper Rhine valley about 170 km northeast of Freiburg. Hourly measurements have been performed by the Institut für Umweltphysik, University of Heidelberg (Levin et al., 2002) at 20 m above the ground. The meteorological conditions during summer in Freiburg and at Schauinsland have characteristics of complex terrain, as studied in SLOPE (Kalthoff et al., 2000; Fiedler et al., 2000) and are different from typical continental sites. During winter, the meteorological situation is characterized by low, persistent stratus decks associated with stable conditions (Dentener et al., 1999).

We have applied here two corrections to the ^{222}Rn measurements from Freiburg used in previous studies, one for the ^{220}Rn daughter contribution and the other for disequilibrium between ^{222}Rn and its measured daughters. Both factors have significant effects on the measurements in the ABL. See Appendix for details. After these corrections, mean concentrations in 2002 and 2003 for Heidelberg, Freiburg and Schauinsland are 4.6 ± 3.6, 7.3 ± 4.9, 2.5 ± 1.7 Bq m^{-3}, respectively. Note that in these values, effects related to vertical gradient during nighttime are retained.

On typical days, Freiburg (and Heidelberg) ^{222}Rn shows maximum concentrations at dawn, and minimum concentrations in the early afternoon (Levin et al., 2003; Schmidt et al., 2003; Olivié et al., 2004). Concentrations at Schauinsland have their maximum in the early afternoon and their minimum during late night. Concentrations are compared to each other for two time periods, midnight to dawn (01:00–06:00 UTC) and early afternoon (12:00–17:00 UTC), as illustrated in Fig. 2, which shows frequency distributions of differences of six hour mean concentrations between Heidelberg, Freiburg and Schauinsland. Similar results are obtained for a single hour to a few hours within each time period. In midnight to dawn hours (a) concentrations in Heidelberg and Freiburg are both higher than at Schauinsland. The most frequent difference between Heidelberg and Schauinsland concentrations is about 2 Bq m^{-3}. The differences for Freiburg extend over a much broader range, between 1 to 8 Bq m^{-3}. Much larger differences are more frequently observed in Freiburg than Heidelberg indicating strong nighttime inversions being more frequent in Freiburg. Also the fact that the Freiburg air intake is closer to the ground may contribute to the more elevated ^{222}Rn activities during night. At early afternoon hours (b) concentrations in Heidelberg sometimes agree with Schauinsland to within 0.5 Bq m^{-3}, indicating well mixed conditions in Heidelberg. On the other hand, concentrations in Freiburg are seldom smaller than those at Schauinsland, indicating that a vertical gradient of about 1 Bq m^{-3} remains between Freiburg and Schauinsland even in daytime. The concentration difference between Freiburg and Heidelberg is also inconsistent with tower observations (Moses et al., 1960; Servant, 1966) which suggest that the concentrations at 8 m and at 20 m are indistinguishable in convective conditions. However the data show that concentrations in Heidelberg (20 m) are lower than in Freiburg (8 m) even at daytime. One could explain the horizontal gradient by assuming higher exhalation rate around Freiburg due to soil type, but this cannot explain the vertical

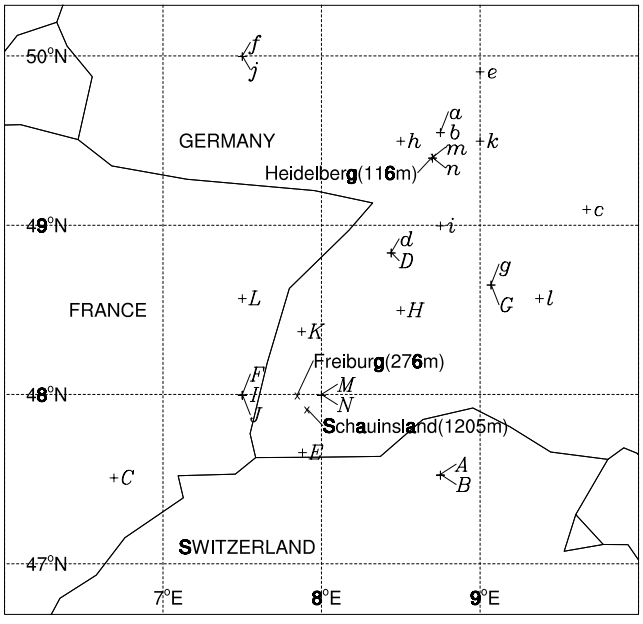

Fig. 1. Locations of Freiburg, Heidelberg and Schauinsland measurements along with the sampling locations of each model (letters). Capital letters are the model locations representing Freiburg and Schauinsland, lower case letters represent Heidelberg. See Table 1 to identify the model corresponding to each letter.

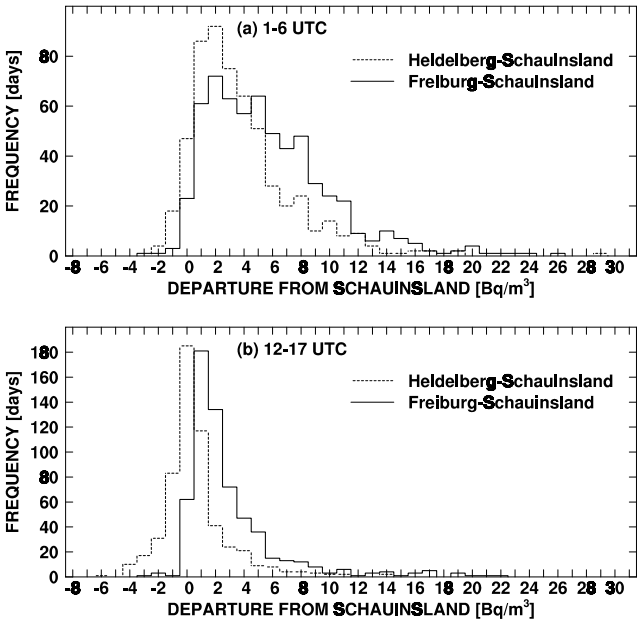

Fig. 2. Frequency distributions of departures of concentrations in Heidelberg and Freiberg from Schauinsland averaged over **(a)** midnight to dawn hours (01:00 to 06:00 UTC) and **(b)** afternoon hours (12:00 to 17:00 UTC); solid line for Freiburg minus Schauinsland, dashed line for Heidelberg minus Schauinsland.

gradient. One alternative explanation is the local low level inversion resulting from a cold air pool from the Rhine valley (Kalthoff et al., 2000; Fiedler et al., 2000). There are two inversion layers over the Schauinsland region in SLOPE, one at 2 km and a lower one at 1 km. The upper one may be a typical inversion layer represented in the meteorological data set used in the models. The lower one is detected in the valley between Freiburg and Schauinsland and may be extended over or near Freiburg suppressing vertical diffusion. There is no information regarding such a low level inversion in Heidelberg.

2.2 Boundary layer height

Boundary layer thickness diagnosed in the European Centre for Medium Range Weather Forecasts (ECMWF) numerical weather forecast system (NWF) was used for a reference BLH. The term, "diagnosed", means that BLH is not a forecast variable, but is calculated after the prediction of atmospheric states. We adopted this BLH because it was available more frequently in NWF systems (3 h) as compared to radiosondes (12 h) and was available at 0.5°, horizontal resolution. The archive of BLH used in this study is different from that used in an earlier study (Olivié et al., 2004) but data were produced in a similar manner. To assess the diagnosed BLH in the ECMWF dataset, we also estimated BLH from radiosonde observations available in the neighborhood (Nancy, Hanau, Stuttgart, Sigmaringen), defining the BLH as the height at which potential temperature is the same as the surface when the lowest layer is unstable. We computed hourly BLH at observational sites using interpolation in time and space from the diagnosed BLH at forecast times of 12, 15, 18, 21 h starting at 00:00 and 12:00 UTC (http://www.ecmwf.int/research/ifsdocs/CY33r1/index.html, Sect. 3.12.1). We found reasonable correlation between the radiosonde and ECMWF BLHs except at Sigmaringen which had relatively few radiosondes available in 2002–2003. The local low level inversion studied in the SLOPE experiments (Kalthoff et al., 2000; Fiedler et al., 2000) was not used in this study because the horizontal scale of the low level inversion may be smaller than the grid interval of the meteorological data used.

3 Participating models and the experiment

The fourteen models, or model variants, used in this analysis are a subset of models collected in TransCom and are listed in Table 1. Six models are on-line, i.e. meteorology is generated as part of the model simulation with winds (and in two cases, temperature) nudged towards National Center for Atmospheric Research (NCAR) and National Center for Environmental Prediction (NCEP) reanalysis (Kalnay et al., 1996). Eight models are off-line, with meteorological forcing provided by ECMWF, Goddard Earth Observing System Data Assimilation System (GEOS DAS) or NCAR/NCEP. All models analyzed here reported BLH, although configuration and inplementations of the boundary layer differ between models. For vertical coordinates, eight models have pressure-sigma hybrid levels. Five models have sigma coordinates. One model, NICAM, has a height-based terrain following coordinate. Modelers chose the horizontal positions to report simulated concentrations; either from a nearest grid point value, or interpolated to the site location from values at surrounding grid points as shown in Fig. 1. Lower case letters correspond to Heidelberg. Capital letters correspond to Freiburg and Schauinsland. Note that two models sampled their output at the same locations (d and D, g and G). The lowest model level concentrations were always used for Freiburg and Heidelberg. For Schauinsland, a vertical interpolation was made using a common scheme as described below.

Compared to the WMO inter-comparison (Rasch et al., 2000) in which 15 models participated, spatial resolutions have increased from 2.5°–10° to 1.0°–2.8° in the horizontal and from 9–21 to 18–60 layers in the vertical. As mentioned before, all on-line models in this study are forced with the observed meteorological fields, which was not the case in the previous inter-comparison where the focus was only on seasonal time-scales.

Table 1. List of participating models with selected properties. On/Off indicates that the model is run with the calculation of wind fields (On) or without them (Off). Meteorological data set to drive transport is indicated in the abbreviation of the organization which produced the data set. Horizontal resolution is shown either in degrees or length. Vertical levels are indicated with number of levels and the type of coordinates;σ indicates that the vertical levels are defined with the ratio of pressure at the level and a reference. η is for hybrid of pressure and σ. "z" indicates the vertical levels are altitude without temporal variations. See Law et al. (2008) for organizations which provided output. Also see the references at the end of each line for details.

#	On/ Off	Meteor data	Horizontal resolution	Vertical levels	Model Name	Reference
A	On	NCEP	$2.5° \times 2.0°$	24η	AM2	GFDL (2004)
B	On	NCEP	$2.5° \times 2.0°$	24η	AM2t	GFDL (2004)
C	On	NCEP	208 km	18σ	CCAM	Law et al. (2006)
D	On	NCEP	$2.8° \times 2.8°$	32σ	CCSR_NIES1	Patra et al. (2009)
E	On	NCEP	$1.1° \times 1.1°$	32σ	CCSR_NIES2	Patra et al. (2009)
F	Off	GEOS4	$2.5° \times 2.0°$	55η	IMPACT	Rotoman et al. (2004)
G	On	NCEP	240 km	54z	NICAM	Satoh et al. (2008)
H	Off	NCEP	$1.0° \times 1.0°$	47σ	NIES	Maksyutov et al. (2008)
I	Off	GEOS4	$1.25° \times 1.0°$	25η	PCTM(CSU)	Kawa et al. (2004)
J	Off	GEOS4	$2.5° \times 2.0°$	25η	PCTM(GSFC)	Kawa et al. (2004)
K	Off	ECMWF	$1.125° \times 1.125°$	60η	STAG	Wada et al. (2007)
L	Off	NCEP	$2.8° \times 2.8°$	28σ	STAGN	Sawa et al. (2007)
M	Off	ECMWF	$3° \times 2°$ ($1° \times 1°$ Europe)	25η	TM5_eur1x1	Krol et al. (2005)
N	Off	ECMWF	$3° \times 2°$	25η	TM5_glb3x2	Krol et al. (2005)

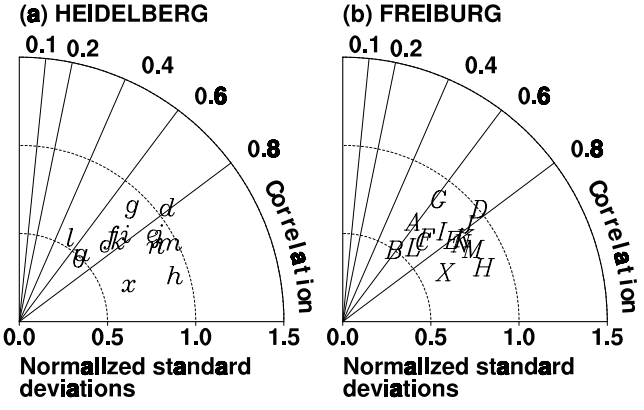

Fig. 3. Taylor diagram for boundary layer height referred to products of European Centre for Medium Range Weather Forecasts in Heidelberg **(a)** and Freiburg **(b)**. Letters represent each model listed in Table 1.

Each model simulated global concentrations of ^{222}Rn using a common flux distribution for four years (Law et al., 2008). The flux over land between 60° S–60°N was set to 1.66×10^{-20} mol m^{-2} s^{-1}. No temporal variations were considered. Simulation results in the first two years were discarded as spin up time. Hourly model concentrations in the last two years (2002, 2003) were submitted for 100 locations at vertical levels up to around 500 hPa for each model. Associated meteorological values were also submitted.

4 Results

4.1 Boundary layer height

Hourly variations of BLH in terms of altitude above the mean sea level at Heidelberg and Freiburg (and Schauinsland) are compared with those provided from ECMWF. Figure 3 shows Taylor diagrams (Taylor, 2001) of BLH where correlation is shown by the angle from the vertical axis and the size of variations by the radial distance. Letters correspond to each model listed in Table 1 except "x" which corresponds to an ensemble average of BLH of all models.

Model H has the highest correlations followed by model M and N. The reason for the high correlations of these models is that they explicitly used BLH provided from ECMWF, though details of BLH in these models and the present study are not exactly the same. For example, one difference is that M and N used constant BLH for 3 h while we used hourly BLH from temporal interpolation of the ECMWF forecast for comparison. Some models with low correlations, such as (l) in Fig. 3a, are sampling data at the largest distance to Heidelberg as shown in Fig. 1. Models (A) and (B) showing smaller correlations in Fig. 3b, are also sampling values remote from Freiburg (Fig. 1). The ensemble average of all models (x) shows higher correlations compared to most models probably because BLH used in models were distributed around the reference BLH estimated at exact locations of Heidelberg and Freiburg in Fig. 1. Therefore, it is suggested that the sampling point of each model may modify the score

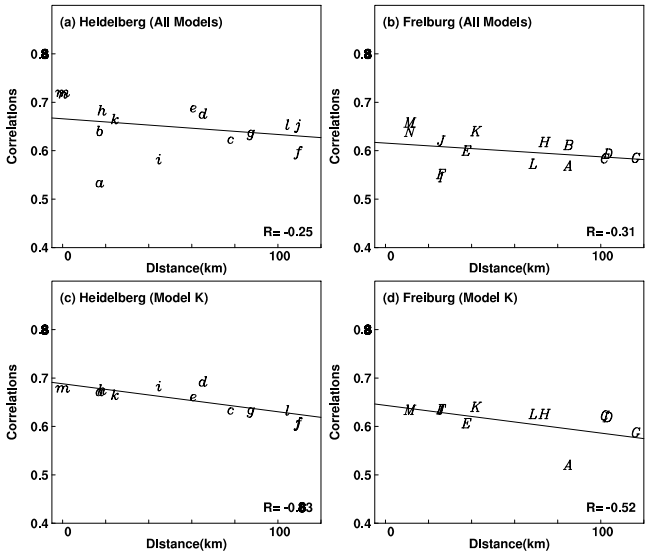

Fig. 4. Correlations between simulations and measurements of hourly concentrations of ^{222}Rn and the distance of sampling point from the monitoring site for **(a)** Heidelberg JJA 2002, **(b)** Freiburg JJA 2002. Correlations from model K for Heidelberg JJA 2002 **(c)** and for Freiburg JJA 2002 **(d)**. See text for details. Where sampling locations are the same for different models only one letter is shown.

of each model, such as correlation (Sect. 4.2), mismatch and normalized standard deviations. To evaluate each model, it may be better to distinguish the effect of sampling location from the total performance of the model. The method used to define BLH in each model may also contribute to the differences from the ECMWF derived BLH. The other point suggested from Fig. 3 is that by making the ensemble average of models, the score is higher; errors in the simulated signal are reduced by averaging. We will assume this effect in the following discussions.

4.2 Correlation of hourly concentrations

The effect of sampling location is investigated for concentrations of ^{222}Rn. Figure 4 shows the correlation between simulated and measured concentrations for individual models at the surface sites along with the distance of each model's sampling location from the site. Two cases (a) Heidelberg in JJA 2002 and (b) Freiburg in JJA 2002 are shown as examples. Seasonal mean correlations are distributed around 0.6 with a weak dependency on the distance between the model sampling location and the site. We also made correlations using one model's (K) output sampled by linear interpolation at the locations of the sampling points of the other models (Fig. 1). This confirms, for a single model, the dependence of seasonal mean correlation on distance solely from horizontal distributions of concentrations without heterogeneous flux distribution, a complication when the evaluation used CO_2 (Patra et al., 2008). Figure 4c demonstrates the disadvantage for a specific location (A) where seasonal mean correlation in model K is far less than the regression line. This disadvantage indicates a type of site effect at the point due to air flow over complex terrain. Therefore, we conclude that the sampling location has a small but detectable effect on the evaluation of model performance and future inter-comparisons might therefore recommend sampling model output for inland sites as close to the observations as possible, i.e. by interpolation. By contrast, Law et al. (2010) noted that interpolation is a poor choice for sampling coastal sites.

4.3 Positioning of simulated concentrations at Schauinsland

Because we collected concentrations and pressure of each level in individual models, we could derive concentrations at any station altitude. We compared the model ^{222}Rn concentrations at each altitude in the model to the observed concentrations at Schauinsland (1205 m) using hourly data in Fig. 5. Concentrations at the site altitude were estimated using an interpolation based on pressure value at each model level. As a reference, hourly pressure at the altitude of Schauinsland was estimated from 6 hourly ECMWF operational analyses using linear interpolation in time and space. Concentrations at Schauinsland at this reference pressure were estimated from the vertical profile of simulated concentrations of each model.

The standard deviation of the simulated concentrations is plotted in a bold solid curve in the left side of each panel of (Fig. 5). It is normalized with the standard deviation of measured concentration (N.S.D.). All models show a steep decrease with altitude up to the station altitude, indicated with an arrow. At the station altitude, the normalized standard deviations of models (B) and (L) are about one, meaning the size of variations corresponds well with the observations. The size of variations is underestimated in other models.

The correlations are shown at the altitude of each model level. Since hourly concentrations are used in the calculations, the correlations include diurnal to seasonal variations as seen by Patra et al. (2008). We obtained the largest correlations at or slightly below the altitude of the site. Based on the correlation profile shown in Fig. 5, we use the modelled concentrations interpolated to the altitude of Schauinsland for comparing with observations. However, given the generally low N.S.D.s at the site altitude, we also test the sensitivity to sampling the models at a lower altitude of 800 m.

4.4 Mean model characteristics

We have computed the ensemble mean of model outputs by averaging the 14 models at each hourly time step and have compared this ensemble mean with the measured concentrations at each hour. Monthly averages and standard deviations

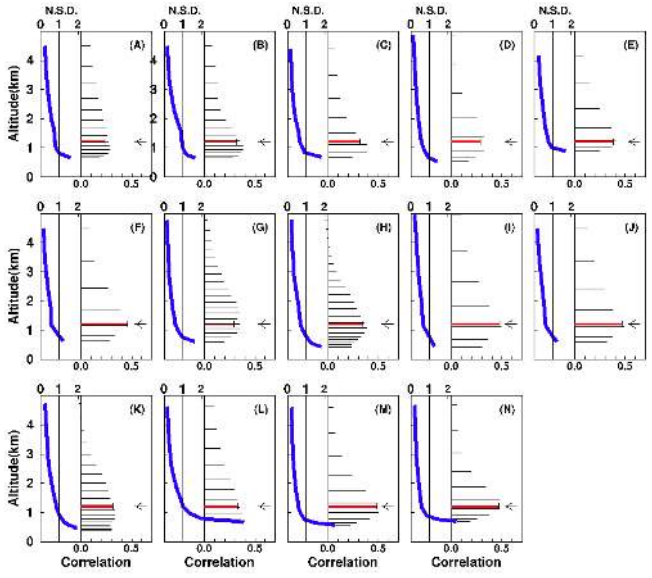

Fig. 5. Vertical profile of normalized standard deviation (N.S.D.) and correlation of simulated to measured concentrations at Schauinsland. Each panel corresponds to a model listed in Table 1. In each panel, N.S.Ds are plotted on the left side (blue). Correlations between simulated and measured concentrations are shown in the right hand side of a panel. Altitude of Schauinsland is indicated by an arrow in each panel. Correlations at the altitude is indicated with the red bar.

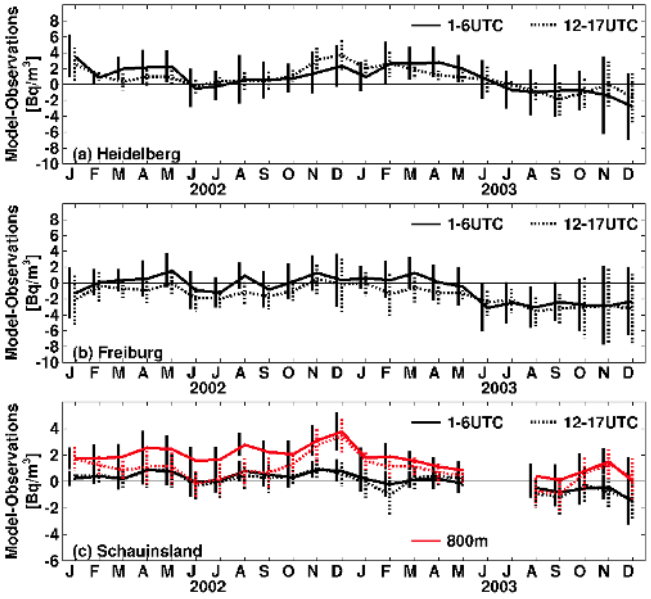

Fig. 6. Monthly mean and standard deviations of mismatch defined as simulated minus measured concentrations for Heidelberg **(a)**, Freiburg **(b)** and Schauinsland **(c)** estimated in midnight to dawn hours (01:00–06:00 UTC, dashed line) and in afternoon hours (12:00–17:00 UTC, solid line) for 2002 and 2003. Measured concentrations are subtracted from the ensemble mean of fourteen model outputs. Vertical line indicates one standard deviation of 6 hourly mean of mean model. Statistics obtained at 800 m are shown in red.

of the hourly mismatch (mean simulated concentrations minus measured concentrations) averaged over two six hour time periods are shown in Fig. 6 for 2002 and 2003. The solid curve shows an average of the mismatch for early afternoon hours. Note that the mismatch is calculated only when the measured concentrations are available. The error bar corresponds to one standard deviation. The same statistics were calculated separately for midnight to dawn hours (01:00–06:00 UTC) and are shown as the dashed line.

In Heidelberg (Fig. 6a), the mean-model overestimates the measurements mostly for winter and spring months, both in afternoon hours and midnight to dawn hours. For afternoon hours, the typical measured concentrations are only about 2 Bq m^{-3} even in winter. Therefore, simulated concentrations are twice as high compared to measured concentrations. These differences can be explained by the constant radon flux used in the model simulations. This flux is close to the magnitude of the flux around Heidelberg in summer (Schmidt et al., 2003) but much larger than the winter flux.

By contrast, at Freiburg (Fig. 6b), the models underestimate the measured concentrations in summer seasons, especially during afternoon hours in terms of one standard deviation of daily mean of the mean model. The overestimate at Heidelberg and the underestimate at Freiburg are consistent with the large differences in measured concentrations between the two sites, given the fact that these two sites are typically separated only by one grid cell in the models.

At Schauinsland (Fig. 6c), the model mean simulated the measured concentrations within the one standard deviation range, while mean discrepancies are negative after July 2003. Note that the vertical axis for Schauinsland (Fig. 6c) is different from Heidelberg (Fig. 6a) and Freiburg (Fig. 6b). If 800 m sampling is used instead of 1205 m sampling, the model-data mismatch is more positive, especially for nighttime hours all year and daytime hours in winter. This would be consistent with the Heidelberg result which suggested the radon flux used in this experiment was too large in winter. The temporal evolution of the model-data mismatch is consistent over both sampling heights.

Because measured concentrations in Heidelberg are very similar to measured concentrations at Schauinsland, we may regard the high concentrations at Freiburg as sub-grid phenomena not suitable for testing atmospheric transport models that do not resolve local low level inversion layer. The measured concentrations at Freiburg may provide a challenging test bed for atmospheric transport models which resolve complex terrain and stable layers (Fiedler et al., 2000).

Despite the differences in the mean mismatches, there is a temporal variation common to all sites. Mismatches decrease

in 2003 and are persistently negative at all three sites after July 2003. This is due to an increase in the observed concentrations rather than a decrease in the simulated ones. We might imagine at least three possibilities to explain this feature. The first is a temporal change of local mixing strength that is poorly resolved in the global transport models. This seems unlikely; we have compared boundary layer heights of ECMWF in this region between 2002 and 2003, and there is no evidence that these have changed significantly in the latter half of 2003. The second possibility is spatial differences in emissions (which were ignored in the experiment) combined with changing dominant transport pathways. The third possibility is temporal variations in the ^{222}Rn exhalation rate. These two emissions-related possibilities are considered briefly in Sect. 5.2.

4.5 Vertical and horizontal gradient of daytime concentrations

We have investigated horizontal as well as vertical gradients of simulated and measured concentrations for early afternoon hours. Figure 7 shows concentrations in Heidelberg minus concentrations at Schauinsland (sampled at both 1205 m and 800 m). The first decile, the first quartile, the median, the third quartile and the ninth decile are shown with box and whisker for observations (O) and for each model (A–N). Statistics for models were derived from only hours when the measured concentrations are available. We also derived these statistics for different hours within early afternoon hours and obtained similar characteristics.

The measured concentrations (O) agree each other as was already shown in Fig. 2. On the other hand, simulated concentrations in Heidelberg agree with those at Schauinsland less frequently when sampled from the models at 1205 m, i.e. the median is located above the zero line for all models except D and G. Note that D and G reported surface concentrations in Heidelberg and the vertical profile for Schauinsland from the same grid point (Fig. 1) and their results show that, for these models, the radon concentration always decreases with height within a grid-cell column.

The models agree better with the observations when sampled at 800 m. In this case the median Heidelberg-Schauinsland (HEI-SCH) difference is closer to zero and some models show a proportion of negative differences, similar to those seen in the observations. With the exception of models K and L, the range of HEI-SCH differences is smaller than observed, but given that the models are likely sampling neighbouring grid-cells to represent HEI and SCH, this would be expected. Models also implicitly average over small scale features within a grid-box which reduces their variability.

The better agreement for HEI-SCH differences when sampled at 800 m compared to 1205 m is consistent with underestimating N.S.D. at 1205 m (shown in Fig. 5) but is not consistent with seeing better correlations with the observations

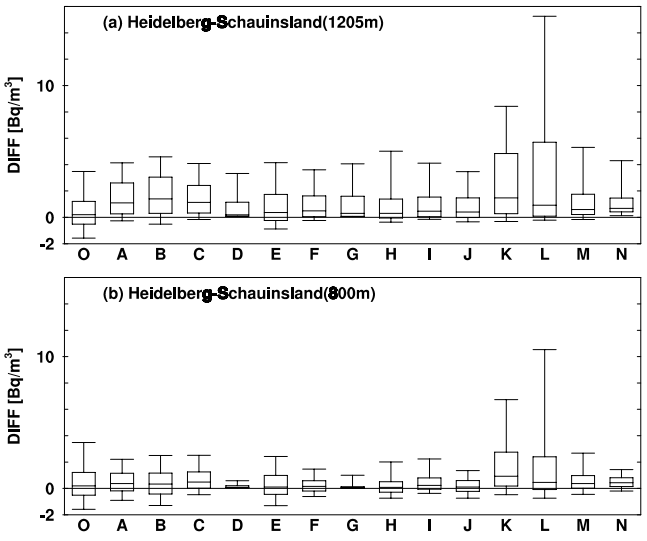

Fig. 7. Departure of six hour (12:00–17:00 UTC) concentrations of Heidelberg from those at Schauinsland. Measurements are indicated with "O". Departures in each model are indicated with letters as listed in Table 1. The first decile, the first quartile, the median, the third quartile and the ninth decile are shown with box and whiskers. Concentrations at Schauinsland are sampled at both 1205 m **(a)** and 800 m **(b)**.

when sampling closer to 1205 m. One possible reason for the difference is that the correlation is driven by synoptic variations in radon which are driven by meteorology, and sampling the models close to 1205 m gives a better representation of the meteorology observed at the site location. However, the median radon concentration and magnitude of variability (as measured by N.S.D.) is driven by the input flux. For the observations, the site is at the surface and close to the input flux, while sampling the models at 1205 m is further from the input flux and median concentrations become too small.

4.6 Diurnal amplitude of boundary layer height and mean concentrations

Seasonal mean concentrations and seasonal mean BLH amplitudes in Heidelberg are shown in Fig. 8 for 2002. BLH amplitude is defined as the difference between the daily maximum BLH and the daily minimum BLH. Mean simulated concentrations are normalized by the measured concentrations. Most models showed concentrations from half to twice the measured mean concentration dependent on season. In all seasons except JJA (c), most models overestimated the measured concentrations. In JJA (c), mismatches are distributed above and below the measured concentrations. These seasonal variations are consistent with Fig. 6.

There are systematic mismatches if we group models by the wind fields used. As listed in Table 1, three groups of models are defined based on their forcing data; models F, I,

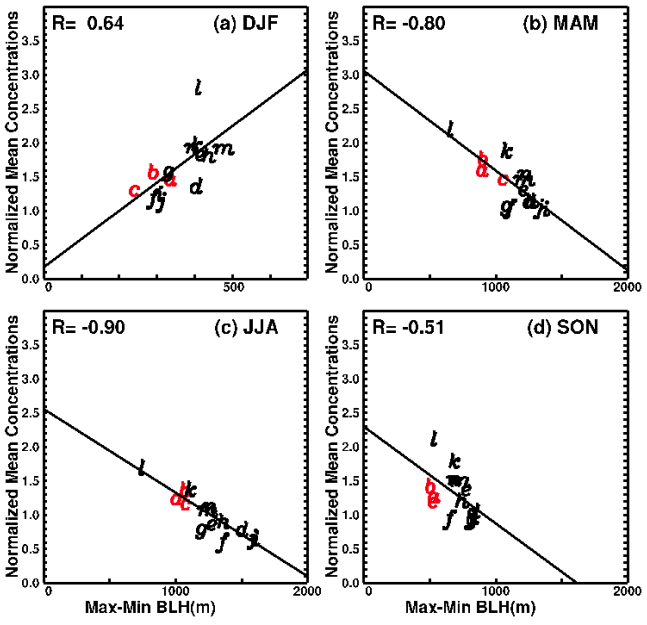

Fig. 8. Scatter plot showing seasonal mean of simulated concentrations divided by measured concentrations and seasonally averaged diurnal amplitude of boundary layer height in Heidelberg in 2002. Correlations and regression line were estimated for each season **(a)** December, January and February, **(b)** March, April and May, **(c)** June, July and August, and **(d)** September, October and November. Each letter corresponds to a model listed in Table 1. See text for details of seasonal variations of a group **(a, b, c)** colored in red.

J use the GEOS4 data set, models K, M, N use the ECMWF data set, and the remaining models use the NCEP data set. Models using the GEOS4 data set are observed at the lower end of the distribution in all seasons. Models using ECMWF data set are observed in the upper part of the distributions. The remaining models are distributed in between, except for model L. A group of models (A, B and C) are located in the lower part of the distributions in DJF (a) and in the upper part in JJA (c). Therefore seasonal variations are smaller than the model mean. If we assume that the ^{222}Rn exhalations at regional scale have no significant seasonal variations, we may conclude that the models other than A, B, C might produce artificial seasonal variations in the mismatch. On the other hand, if we assume that exhalation has a significant seasonal variation, we may conclude that the seasonal variations in the mismatch are reasonable. This contrast demonstrates the crucial value of seasonal variations of exhalation at regional scale.

The most prominent feature in Fig. 8 is the suggestion of a linear relationship between mismatch and BLH which changes with season. The correlations are positive for winter (a) but negative for other seasons. Analysis for Freiburg also gives a positive correlation for winter and negative in other months though the correlations are slightly weaker than for Heidelberg. Schauinsland gives close to zero correlatoin for winter and negative correlations in other seasons. Also note that the diurnal amplitude of boundary layer height is much smaller in winter than in the other seasons. We will try to interpret these characteristics in the next section because the effect of ventilation is not well explored so far.

5 Discussion

5.1 Conceptual relationship between boundary layer height and mean concentrations

Let us consider a simple box model of the boundary layer to understand the phenomena happening in the global models. We may admit that the explanation given here is only speculative and qualitative because all details in the real boundary layers irrelevant to our interests are omitted.

We assume that the ^{222}Rn is well mixed throughout the boundary layer immediately after exhalation from the ground and that mixing between this boundary layer and the free troposphere is prohibited except in the growing and dissipating process. The concentration above the top of the boundary layer is set to zero. In the growing process, the atmosphere above the top of the boundary layer is entrained into the boundary layer. At the dissipating stage, usually in late afternoon, a stable inversion layer may build up below the residual layer. We assume that air in the upper part of the boundary layer above this inversion layer is disconnected from the lower part of the boundary layer. The upper part is diluted immediately to zero concentration in the free troposphere. This process is described using a top-hat function that is a simplified shape of the boundary layer shape shown in Fig. 9, namely the lower height (h_l) and upper height (h_x) is constant. The start and end time of the upper height (h_x) is denoted by i_s and i_e respectively. The boundary layer height at hour i, $(0 \le i < 24)$ may be written as

$$h(i) = \begin{cases} h_x & (\text{if } i_s \le i \le i_e) \\ h_l & (\text{if } i < i_s, \text{or } i > i_e). \end{cases} \quad (1)$$

By omitting the effect of radioactive decay we may write the mass of ^{222}Rn per unit area in the boundary layer as

$$m(i) = \begin{cases} m(i-1) + f & (\text{if } i \ne i_e + 1) \\ m(i-1)h_l/h_x + f & (\text{if } i = i_e + 1) \end{cases} \quad (2)$$

where the flux from the ground (f) is constant. The mixing ratio of ^{222}Rn in the boundary layer is

$$c(i) = m(i)/h(i) \quad (3)$$

where the coefficients for dimensional volume mixing ratio are omitted for simplicity.

Four types of diurnal evolutions of $m(i)$ and $c(i)$ are numerically calculated and are shown in Fig. 10 using different sets of ABL evolutions in terms of (h_l), (h_x), (i_s) and (i_e). The combination of values for each run is (a) 200, 500,

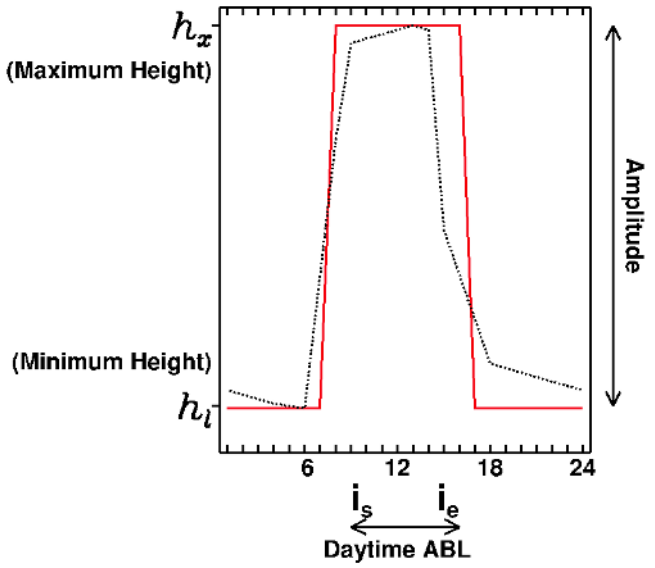

Fig. 9. Factors characterizing the time evolution of boundary layer thickness. Minimum height, maximum height, amplitude are indicated for top-hat shape (red).

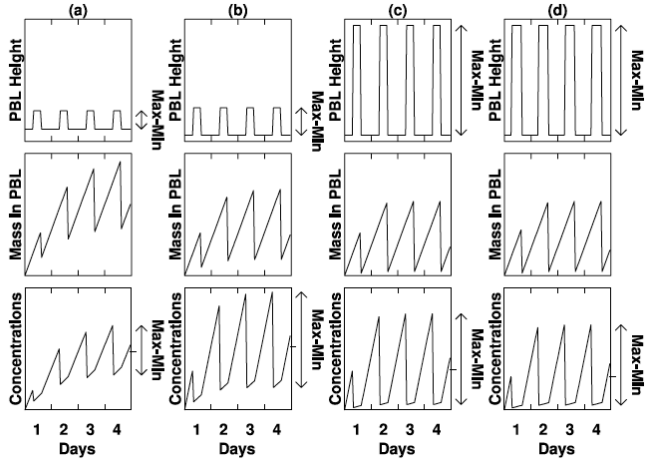

Fig. 10. Boundary layer height and concentrations calculated using our one dimensional model, as described in section 5.1. Top panels show four variations of diurnal cycle of boundary layer height over four days. Middle panels show four days of changes of total ^{222}Rn in the boundary layer assuming a constant source from the bottom. Bottom panels show mixing ratio in the boundary layer assuming homogeneous mixing ratio in the boundary layer and entrainment of free tropospheric air during growing period only. From left to right, four cases are selected to show the relative change of concentration in a day to the change of diurnal variations of boundary layer height. The concentrations in the boundary layer were calculated using Eq. (3). See text for details.

9, 15, (b) 100, 550, 9, 15, (c) 100, 1900, 9, 15, (d) 100, 1900, 8, 16, respectively, with common value f=100. From (a) to (c), (h_l) and (h_x) were modified. From (c) to (d), (i_s) and (i_e) were modified. Diurnal variations of concentrations are almost cyclically stationary by the fourth day in Fig. 10. In the right side of the bottom panel, mean concentrations and maximum minus minimum concentrations are indicated. The mean concentrations and the maximum minus minimum concentrations, (also standard deviation), at day four are increased from (a) to (b) where the nocturnal BLH is reduced and the daytime BLH is increased.

From the case (a) to (b) in Fig. 10, mean concentrations are slightly increased in (b). This phenomenon suggests one possibility to explain the positive correlation between the mean concentration and amplitude of BLH in DJF (Fig. 8a). On the other hand, mean and max-min concentration are decreased from (b) to (c), due to increased daytime BLH, or (c) to (d), due to increased duration of daytime high BLH. These distinctions may explain the trends in the other seasons in Fig. 8.

Nocturnal BLH has both positive and negative effects on daytime concentrations, as demonstrated in the case (a) and (b). As BLH is reduced at nighttime, concentrations in the nighttime are increased and potentially make daytime concentrations higher. At the same time, if the nocturnal BLH is lower, due to an increase in ventilation for the same BLH in daytime, loss due to that ventilation is increased, which potentially reduces the subsequent daytime concentrations. The daily mean concentrations are a result of the balance between these two effects and beyond the scope of the current simplified model.

5.2 Emissions

If we assume that the transport and mixing are represented in the models correctly, one way to explain the temporal variations of the mismatch shown in Figs. 6 and 8 is to relax the condition of a constant flux over Europe. Horizontal as well as temporal variations have the potential to explain the mismatch. We first tested the effect of the change of large scale transport using tagged simulations from $30^\circ \times 30^\circ$ regions over Europe to determine the so called foot print or catchment area of the site. Enhanced emissions in southwestern Europe (Szegvary et al., 2007, 2009) might influence the site occasionally. However these tagged simulations (using model K) show that more than 80 % of concentrations in Heidelberg and Freiburg are caused by ^{222}Rn emitted from a $30^\circ \times 30^\circ$ region around the sites in all seasons. Therefore, we may conclude that high emissions from Southeastern Europe are unable to explain the temporal variations at the three sites under investigation.

The second option to adjust model concentrations to the observations is to introduce temporally changing emissions. For example, the model concentration in Heidelberg may be closer to the observation if we reduce the emission to half of the current value between January to May 2002 and between

November 2002 to May 2003. If we increase the emissions after July 2003, model concentrations become closer to the measurements at all sites. Seasonal changes in flux have been observed in the Heidelberg region (Dörr and Münnich, 1990), consistent with the seasonality in modelled mismatch. This seasonality is thought to be driven by changes in soil moisture, which could also provide a mechanism for interannual changes in radon flux. We have used NOAA Climate Forecast Data System dataset (Saha et al., 2010) to give a time series of soil water content for Heidelberg for 2000–2006 and find that soil water content is above average in 2002 and below average in the second half of 2003 (due to the European summer heatwave and drought that year). This would be consistent with lower radon fluxes in 2002 and higher ones in late 2003. Griffiths et al. (2010) incorporate temporal changes in soil moisture into their estimates of Australian radon fluxes. It may be appropriate in future work to apply a similar process to estimate temporal changes in European fluxes. This result does suggest that some care may be required in flux estimation methods where the flux of a second species is estimated assuming a known radon emission with no interannual variations (Schmidt et al., 2003; Hirsch, 2007).

6 Conclusions

Temporal variations of ^{222}Rn concentrations at three European inland stations were studied using hourly concentrations from simulations and measurements. We found that differences in measured daytime concentrations among these stations were poorly reproduced by the model. Concentrations in Heidelberg and at Schauinsland are almost identical in daytime while models showed small but significant gradients between these sites. While the measured concentrations in Freiburg are higher than those at Schauinsland by about $2\,\mathrm{Bq\,m^{-3}}$ during daytime observations, models show less than $1\,\mathrm{Bq\,m^{-3}}$ gradient. Seasonal mean of simulated concentrations are correlated with the seasonal mean daily amplitudes of boundary layer height in spring, summer and autumn with a sign change for winter compared to the other seasons.

From the simulation and measurement mismatch of concentrations, we may speculate that the emissions are changing with time at regional scale beyond the chamber measurements scale if we assume transport and mixing are reasonably modelled. From correlations between simulated and measured radon, we have confirmed previous findings that correlations depend weakly on the distance between model sampling site and observational site due to concentration distributions caused by transport and mixing. Choosing an appropriate sampling height for mountain sites remains difficult with the radon simulations agreeing better with observations at different sampling heights, depending on the element of the observations being compared.

Due to a lack of effective boundary layer height observations and insufficient ^{222}Rn flux observations over Europe in 2002 and 2003, we were unable to rank the models. In other words, the models reproduced concentrations within the uncertainty resulting from boundary layer thickness and emissions.

The effect of diurnal variations of boundary layer height on mean concentrations via ventilations has largely been ignored up until now. Unfortunately, boundary layer height observations with high vertical and temporal resolution are less prevalent nowadays as compared to the past when air pollution was a more serious problem. Recent development of laser radar makes it easier to conduct continuous monitoring of boundary layer height. Detailed comparison of boundary layer is expected at these two towns in the future.

Appendix A

Corrections applied to FRB data

A radon monitor measuring total alpha activity (i.e. the Freiburg Monitor) measures the daughters from both ^{222}Rn and ^{220}Rn. Results from an inter-comparison between the Freiburg instrument and the Heidelberg instrument (Levin et al., 2002) performed in Freiburg in August 2002 were used to estimate the ^{220}Rn contributions in the Freiburg measurements. In this inter-comparison project a Heidelberg-type monitor was set up at the Freiburg monitor site. Air was taken at 8 m above the ground. Measurements were made in parallel for a month. Half-hourly measurements of both instruments were very well correlated ($R = 0.98$) with the following relation: $\mathrm{Rn(Heidelberg\_Monitor)} = 0.80\,\mathrm{Rn(Freiburg\_Monitor)} - 0.23$. The difference between the two measurements is attributed to the contribution of the ^{220}Rn daughter activity in the Freiburg Monitor measurement which is excluded in the Heidelberg_Monitor measurements (Levin et al., 2002).

The second factor is due to disequilibrium. Vertical profiles of natural radio nuclides, such as ^{214}Po (one of the progenies of ^{222}Rn, i.e. measured in the Heidelberg and in the Schauinsland Monitor) and ^{222}Rn, in the equilibrium state in the ABL under various turbulent diffusion coefficients are obtained by solving the diffusion equation (Jacobi and André, 1963). It was shown that the ratio of ^{214}Po and ^{222}Rn itself is not necessarily constant with altitude but varies with the vertical profiles of diffusion coefficients. Although the disequilibrium factor at Schauinsland is shown to be 87 % without precipitation and 74 % with precipitation for a selected wind sector (Xia et al., 2010) we applied a constant disequilibrium factor at each site for simplicity. Here we corrected for disequilibrium by dividing the observed ^{222}Rn by 0.704 ± 0.091 (Levin et al., 2002) in Freiburg and Heidelberg and by 0.847 ± 0.14 for Schauinsland (Schmidt et al., 2001). Altogether, we thus corrected the Freiburg values as

follows: FRB_new = 1.14FRB_old − 0.33, where FRB_new refers to the values used in this study and FRB_old refers to the original value.

Acknowledgements. The TransCom-continuous model simulations were provided by AM2/AM2t (S. Fan, S.-J. Lin), CCAM (R. M. Law), CCSR_NIES (P. Patra, M. Takigawa), IMPACT (D. J. Bergmann, P. J. Cameron-Smith), NICAM (Y. Niwa, R. Imasu, M. Satoh), NIES05 (S. Maksyutov, R. Onishi), PCTM.CSU (R. Lokupitiya, A. S. Denning, N. Parazoo, J. Kleist), PCTM.GSFC (S. R. Kawa, Z. Zhu), STAG/STAGN (S. Taguchi), TM5_glb3x2 (W. Peters, L. Bruhwiler), TM5_eur1x1 (M. C. Krol, S. Houweling). These data are available by ftp from ftp oaxaca.la.asu.edu (Username: carbon, password: carbon). Many thanks to Kevin Gurney and the Department of Earth and Atmospheric Sciences at Purdue University and the School of Life Sciences, Arizona State University for data handling and ftp site hosting. Individual modeling groups acknowledge the following support. CCAM: Part of this work was supported through the Australian Greenhouse Office. We thank John McGregor and Eva Kowalczyk for their development of CCAM. LLNL: The LLNL portion of this work was performed under the auspices of the US Department of Energy (DOE) by the University of California, Lawrence Livermore National Laboratory (LLNL) under Contract No. W-7405-Eng-48. The project (06-ERD-031) was funded by the Laboratory Directed Research and Development Program at LLNL. This work and PKP are partly supported by the Grants-in-Aid for Creative Scientific Research (2005/17GS0203) of the Ministry of Education, Science, Sports and Culture, Japan.

Edited by: P. Jöckel

References

Allen, D. J., Rood, R. B., Thompson, A. M., and Hudson, R. D.: Three-dimensional radon 222 calculations using assimilated meteorological data and a convective mixing algorithm, J. Geophys. Res., 101, 6871–6881, 1996.

Chevillard, A., Ciais, P., Karstens, U., Heimann, M., Schmidt, M., Levin, I., Jacob, D., Podzun, R., Kazan, V., Sartorius, H., and Weingartner, E.: Transport of ^{222}Rn using the regional model REMO: a detailed comparison with measurements over Europe, Tellus B, 54, 850–871, 2002.

Conen, F. and Robertson, L. B.: Latitudinal distribution of radon-222 flux from continents, Tellus B, 54, 127–133, 2002.

Considine, D. B., Bergmann, D. J., and Liu, H.: Sensitivity of Global Modeling Initiative chemistry and transport model simulations of radon-222 and lead-210 to input meteorological data, Atmos. Chem. Phys., 5, 3389–3406, doi:10.5194/acp-5-3389-2005, 2005.

Dörr, H. and Münnich, K. O.: ^{222}Rn flux and soil air concentration profiles in West-Germany. Soil ^{222}Rn as tracer for gas transport in the unsaturated soil zone, Tellus B, 42, 20–28, 1990.

Dentener, F., Feichter, J., and Jeuken, A.: Simulation of the transport of Rn^{222} using on-line and off-line global models at different horizontal resolutions: a detailed comparison with measurements, Tellus B, 51, 573–602, 1999.

Donner, L. J., Horowitz, L. W., Fiore, A. M., Seman, C. J., Blake, D. R., and Blake, N. J.: Transport of radon-222 and methyl iodide by deep convection in the GFDL Global Atmospheric Model AM2, J. Geophys. Res., 112, D17303, doi:10.1029/2006jd007548, 2007.

Fiedler, F., Bischoff-Gauss, I., Kalthoff, N., and Adrian, G.: Modeling of the transport and diffusion of a tracer in the Freiburg-Schauinsland area, J. Geophys. Res., 105, 1599–1610, 2000.

GFDL Global Atmospheric Model Development Team: The new GFDL global atmosphere and land model AM2-LM2: Evaluation with prescribed SST simulations, J. Climate, 17, 4641–4673, doi:10.1175/JCLI-3223.1, 2004.

Griffiths, A. D., Zahorowski, W., Element, A., and Werczynski, S.: A map of radon flux at the Australian land surface, Atmos. Chem. Phys., 10, 8969–8982, doi:10.5194/acp-10-8969-2010, 2010.

Hammer, S. and Levin, I.: Seasonal variation of the molecular hydrogen uptake by soils inferred from continuous atmospheric observations in Heidelberg, southwest Germany, Tellus B, 61, 556–565, doi:10.1111/j.1600-0889.2009.00417.x, 2009.

Heimann, M. and Keeling C. D.: A three-dimnsional model of atmospheric CO_2 transport based on observed winds: 2. Model description and simulated tracer experiments, in: Aspects of climate variability in the Pacific and the western Americas, Geophysical Monograph Series, edited by: Peterson, D. H. , Americal Geophysical Union, Washington, DC, USA, 237–275, 1989.

Hirsch, A. I.: On using radon-222 and CO_2 to calculate regional-scale CO_2 fluxes, Atmos. Chem. Phys., 7, 3737–3747, doi:10.5194/acp-7-3737-2007, 2007.

Holtslag, A. A. M. and Boville, B. A.: Local versus nonlocal boundary-layer diffusion in a global climate model, J. Climate, 6, 1825–1842, 1993.

Jacob, D. J., Prather, M. J., Rasch, P. J., Shia, R. L., Balkanski, Y. J., Beagley, S. R., Bergmann, D. J., Blackshear, W. T., Brown, M., Chiba, M., Chipperfield, M. P., deGrandpre, J., Dignon, J. E., Feichter, J., Genthon, C., Grose, W. L., Kasibhatla, P. S., Kohler, I., Kritz, M. A., Law, K., Penner, J. E., Ramonet, M., Reeves, C. E., Rotman, D. A., Stockwell, D. Z., VanVelthoven, P. F. J., Verver, G., Wild, O., Yang, H., and Zimmermann, P.: Evaluation and intercomparison of global atmospheric transport models using ^{222}Rn and other short-lived tracers, J. Geophys. Res., 102, 5953–5970, 1997.

Jacobi, W. and André, K.: The vertical distribution of radon 222, radon 220 and therdecay products in the atmosphere, J. Geophys. Res., 68, 3799–3814, 1963.

Josse, B., Simon, P., and Peuch, V. H.: Radon global simulations with the multiscale chemistry and transport model MOCAGE, Tellus B, 56, 339–356, 2004.

Kalnay, E., Kanamitsu, M., Kistler, R., Collins, W., Deaven, D., Gandin, L., Iredell, M., Saha, S., White, G., Woollen, J., Zhu, Y., Chelliah, M., Ebisuzaki, W., Higgins, W., Janowiak, J., Mo, K. C., Ropelewski, C., Wang, J., Leetmaa, A., Reynolds, R., Jenne, R., and Joseph, D.: The NCEP/NCAR 40-year reanalysis project, B. Am. Meteorol. Soc., 77, 437-471, 1996.

Kalthoff, N., Horlacher, V., Corsmeier, U., Volz-Thomas, A., Kolahgar, B., Geiss, H., Mollmann-Coers, M., and Knaps, A.: Influence of valley winds on transport and dispersion of airborne pollutants in the Freiburg-Schauinsland area, J. Geophys. Res., 105, 1585–1597, 2000.

Kawa, S. R., Erickson III, D. J., Pawson, S., and Zhu, Z.: Global CO_2 transport simulations using meteorological data from the NASA data assimilation system, J. Geophys. Res., 109, D18312,

doi:10.1029.2004JD004554, 2004.

Krol, M., Houweling, S., Bregman, B., van den Broek, M., Segers, A., van Velthoven, P., Peters, W., Dentener, F., and Bergamaschi, P.: The two-way nested global chemistry-transport zoom model TM5: algorithm and applications, Atmos. Chem. Phys., 5, 417–432, doi:10.5194/acp-5-417-2005, 2005.

Law, R. M., Kowalczyk, A. K., and Wang Y. P.: Using atmospheric CO_2 data to access a simplified carbon-climate simulation for the 20th century, Tellus B, 53, 427–437, doi:10.1111/j.1600-0889.2006.00198.x, 2006.

Law, R. M., Peters, W., Rödenbeck, C., Aulagnier, C., Baker, I., Bergmann, D. J., Bousquet, P., Brandt, J., Bruhwiler, L., Cameron-Smith, P. J., Christensen, J. H., Delage, F., Denning, A. S., Fan, S., Geels, C., Houweling, S., Imasu, R., Karstens, U., Kawa, S. R., Kleist, J., Krol, M. C., Lin, S. J., Lokupitiya, R., Maki, T., Maksyutov, S., Niwa, Y., Onishi, R., Parazoo, N., Patra, P. K., Pieterse, G., Rivier, L., Satoh, M., Serrar, S., Taguchi, S., Takigawa, M., Vautard, R., Vermeulen, A. T., and Zhu, Z.: TransCom model simulations of hourly atmospheric CO_2: Experimental overview and diurnal cycle results for 2002, Global Biogeochem. Cy., 22, GB3009, doi:10.1029/2007gb003050, 2008.

Law, R. M., Steele, L. P., Krummel, P. B., and Zahorowski, W.: Synoptic variations in atmospheric CO_2 at Cape Grim: a model intercomparison, Tellus B, 62, 810–820, doi:10.1111/j.1600-0889.2010.00470.x, 2010.

Levin, I., Born, M., Cuntz, M., Langendorfer, U., Mantsch, S., Naegler, T., Schmidt, M., Varlagin, A., Verclas, S., and Wagenbach, D.: Observations of atmospheric variability and soil exhalation rate of radon-222 at a Russian forest site – Technical approach and deployment for boundary layer studies, Tellus B, 54, 462–475, 2002.

Levin, I., Kromer, B., Schmidt, M., and Sartorius, H.: A novel approach for independent budgeting of fossil fuel CO_2 over Europe by $^{14}CO_2$ observations, Geophys. Res. Lett., 30, 2194, doi:10.1029/2003gl018477, 2003.

Lock, A. P., Brown, A. R., Bush, M. R., Martin, G. M., and Smith, R. N. B.: A new boundary layer mixing scheme. Part I: Scheme description and single-column model tests, Mon. Weather Rev., 128, 3187–3199, 2000.

Mahowald, N. M., Rasch, P. J., Eaton, B. E., Whittlestone, S., and Prinn, R. G.: Transport of ^{222}radon to the remote troposphere using the model of atmospheric transport and chemistry and assimilated winds from ECMWF and the National Center for Environmental Prediction NCAR, J. Geophys. Res., 102, 28139–28151, 1997.

Maksyutov, S., Patra, P. K., Onishi, R., Saeki, T., and Nakazawa, T.: NIES/FRCGC global atmospheric tracer transport model: description, validation, and surface sources and sinks inversion, J. Earth Simulator, 9, 3–18, 2008.

Moses, H., Stehney, A. F., and Lucas, H. F.: The effect of meteorological variables upon the vertical and temporal distribution of atmospheric radon, J. Geophys. Res., 65, 1223–1238, 1960.

Nazaroff, W. W.: Radon transport from soil to air, Rev. Geophys., 30, 137–160, 1992.

Olivié, D. J. L., van Velthoven, P. F. J., Beljaars, A. C. M., and Kelder, H. M.: Comparison between archived and off-line diagnosed convective mass fluxes in the chemistry transport model TM3, J. Geophys. Res., 109, D11303, doi:10.1029/2003jd004036, 2004.

Patra, P. K., Law, R. M., Peters, W., Rödenbeck, C., Takigawa, M., Aulagnier, C., Baker, I., Bergmann, D. J., Bousquet, P., Brandt, J., Bruhwiler, L., Cameron-Smith, P. J., Christensen, J. H., Delage, F., Denning, A. S., Fan, S., Geels, C., Houweling, S., Imasu, R., Karstens, U., Kawa, S. R., Kleist, J., Krol, M. C., Lin, S. J., Lokupitiya, R., Maki, T., Maksyutov, S., Niwa, Y., Onishi, R., Parazoo, N., Pieterse, G., Rivier, L., Satoh, M., Serrar, S., Taguchi, S., Vautard, R., Vermeulen, A. T., and Zhu, Z.: TransCom model simulations of hourly atmospheric CO_2: Analysis of synoptic-scale variations for the period 2002–2003, Global Biogeochem. Cy., 22, GB4013, doi:10.1029/2007gb003081, 2008.

Patra, P. K., Takigawa, M., Dutton, G. S., Uhse, K., Ishijima, K., Lintner, B. R., Miyazaki, K., and Elkins, J. W.: Transport mechanisms for synoptic, seasonal and interannual SF_6 variations and "age" of air in troposphere, Atmos. Chem. Phys., 9, 1209–1225, doi:10.5194/acp-9-1209-2009, 2009.

Rasch, P. J., Feichter, J., Law, K., Mahowald, N., Penner, J., Benkovitz, C., Genthon, C., Giannakopoulos, C., Kasibhatla, P., Koch, D., Levy, H., Maki, T., Prather, M., Roberts, D. L., Roelofs, G. J., Stevenson, D., Stockwell, Z., Taguchi, S., Kritz, M., Chipperfield, M., Baldocchi, D., McMurry, P., Barrie, L., Balkansi, Y., Chatfield, R., Kjellstrom, E., Lawrence, M., Lee, H. N., Lelieveld, J., Noone, K. J., Seinfeld, J., Stenchikov, G., Schwartz, S., Walcek, C., and Williamson, D.: A comparison of scavenging and deposition processes in global models: results from the WCRP Cambridge Workshop of 1995, Tellus B, 52, 1025–1056, 2000.

Rotman D. A., Atherton, C. S., Bergman, D. J., Cameron-Smith, P. J., Chuang, C. C.,Connell, P. S., Dignon, J. E., Franz, A., Grant, K. E., Kinnison, D. E., Molenkamp, C R., Proctor, D. D., and Tannahill, J. R: IMPACT, the LLNL 3-D global atmospheric chemical transport model for the combined troposphere and stratosphere: Model description and analysis of ozone and other trace gases, J. Geophys. Res., 109, D04303, doi:10.1029/2002JD003115, 2004.

Saha, S., Moorthi, S., Pan, H. L., Wu, X. R., Wang, J. D., Nadiga, S., Tripp, P., Kistler, R., Woollen, J., Behringer, D., Liu, H. X., Stokes, D., Grumbine, R., Gayno, G., Wang, J., Hou, Y. T., Chuang, H. Y., Juang, H. M. H., Sela, J., Iredell, M., Treadon, R., Kleist, D., Van Delst, P., Keyser, D., Derber, J., Ek, M., Meng, J., Wei, H. L., Yang, R. Q., Lord, S., Van den Dool, H., Kumar, A., Wang, W. Q., Long, C., Chelliah, M., Xue, Y., Huang, B. Y., Schemm, J. K., Ebisuzaki, W., Lin, R., Xie, P. P., Chen, M. Y., Zhou, S. T., Higgins, W., Zou, C. Z., Liu, Q. H., Chen, Y., Han, Y., Cucurull, L., Reynolds, R. W., Rutledge, G., and Goldberg, M.: The NCEP Climate Forecast System Reanalysis, B. Am. Meteorol. Soc., 91, 1015–1057, doi:10.1175/2010bams3001.1, 2010.

Satoh, M., Matsuno, T., Tomita, H., Miura, H., Nasuno, T., and Iga, S.: Nonhydrostatic icosahedral atmospheric model (NICAM) for global cloud resolving simulations, J. Comput. Phys., 227, 3486–3514, 2008.

Sawa, Y., Tanimoto, H,, Yonemura, S., Matsueda, H., Wada, A., Taguchi, S., Hyasaka, T., Tsuruta, H., Tohjima, Y., Mukai, H., Kikuchi, N., Katagiri, S., and Tsuboi, K.: Widespread pollution events of carbon monoxide observed over the western North Pacific during the East Asian Regional Experiment

(EAREX) 2005 campaign, J. Geophys. Res., 112, D22S26, doi:10.1029/2006JD008055, 2007.

Schery, S. D. and Huang, S.: An estimate of the global distribution of radon emissions from the ocean, Geophys. Res. Lett., 31, L19104, doi:10.1029/2004GL021051, 2004.

Schery, S. D. and Wasiolek, M. A.: Modeling radon flux from the earth's surface, Radon and Thoron in the Human Environment, edited by: Katase, A. and Shimo, M., World Scientific Publ Co Pte Ltd, Singapore, 207–217, 1998.

Schmidt, M., Glatzel-Mattheier, H., Sartorius, H., Worthy, D. E., and Levin, I.: Western European N_2O emissions: A top-down approach based on atmospheric observations, J. Geophys., 106, 5507–5516, 2001.

Schmidt, M., Graul, R., Sartorius, H., and Levin, I.: The Schauinsland CO_2 record: 30 years of continental observations and their implications for the variability of the European CO_2 budget, J. Geophys. Res., 108, 4619, doi:10.1029/2002jd003085, 2003.

Servant, J.: Temporal and spatial variations of the concentration of the short-lived decay products of radon in the lower atmosphere, Tellus B, 18, 663–671, 1966.

Stockwell, D. Z., Kritz, M. A., Chipperfield, M. P., and Pyle, J. A.: Validation of an off-line three-dimensional chemical transport model using observed radon profiles – 2. Model results, J. Geophys. Res., 103, 8433–8445, 1998.

Szegvary, T., Conen, F., Stohlker, U., Dubois, G., Bossew, P., and de Vries, G.: Mapping terrestrial gamma-dose rate in Europe based on routine monitoring data, Radiat. Meas., 42, 1561–1572, doi:10.1016/j.radmeas.2007.09.002, 2007.

Szegvary, T., Conne, F., and Ciais, P.: European ^{222}Rn inventory for applied atmospheric studies, Atmos. Environ., 43, 1536–1539, doi:10.1016/j.atmosenv.2008.11.025, 2009.

Taguchi, S., Iida, T., and Moriizumi, J.: Evaluation of the atmospheric transport model NIRE-CTM-96 by using measured radon-222 concentrations, Tellus B, 54, 250–268, 2002.

Taylor, K. E.: Summarizing multiple aspects of model performance in a single diagram, J. Geophys. Res., 106, 7183–7192, 2001.

Troen, I. W., and Mahrt, I.: A simple model of the atmospheric boundary layer; sensitivity to surface evaporation, Bound.-Lay. Meteorol., 37, 129–148, 1986.

Wada, A., Sawa, Y., Matsueda, H., Taguchi, S., Murayama, S., Okubo, S., and Tsutsumi, Y.: Influence of continental air mass transport on atmospheric CO_2 in the western North Pacific, J. Geophys. Res., 112, D07311, doi:10.1029/2006JD007552, 2007.

Williams, A. G., Zahorowski, W., Chambers, S., Griffiths, A., Hacker, J. M., Element, A., and Werczynski, S.: The vertical distribution of radon in clear and cloudy daytime terrestrial boundary layers, J. Atmos. Sci., 68, 155–174, doi:10.1175/2010jas3576.1, 2011.

Xia, Y., Sartorius, H., Schlosser, C., Stöhlker, U., Conen, F., and Zahorowski, W.: Comparison of one- and two-filter detectors for atmospheric ^{222}Rn measurements under various meteorological conditions, Atmos. Meas. Tech., 3, 723–731, doi:10.5194/amt-3-723-2010, 2010.

Zhang, K., Wan, H., Zhang, M., and Wang, B.: Evaluation of the atmospheric transport in a GCM using radon measurements: sensitivity to cumulus convection parameterization, Atmos. Chem. Phys., 8, 2811–2832, doi:10.5194/acp-8-2811-2008, 2008.